Challenge Journal of CONCRETE RESEARCH LETTERS

Research Article

Structural performance of biaxially-loaded slender hybrid self-compacting concrete columns with RPC shells

Alaa Ali Salman Al-Taai [a,*], Waleed A. Waryosh [a]

[a] *Department of Civil Engineering, Mustansiriyah University, 10052 Baghdad, Iraq*

ABSTRACT

The response of slender hybrid reinforced concrete columns composed of two advanced cementitious composites, self-compacting concrete (SCC) and reactive powder concrete (RPC), under biaxial eccentric compression has not been adequately documented. This study addresses this gap by comparing conventional SCC columns with hybrid SCC columns and examining the development of steel strains and lateral deformations. Six 140 × 140 mm square columns with an overall height of 1260 mm were tested at three eccentricity levels: low, medium, and high. The investigated variables were the outer-shell material, namely self-compacting normal concrete (SC-NC) or self-compacting reactive powder concrete (SC-RPC), and the eccentricity level. In the hybrid specimens, the SC-NC core and SC-RPC outer shell were cast concentrically under fresh-to-fresh conditions to ensure full interaction. The results showed that the use of SC-RPC as the outer-shell material significantly increased the ultimate load and moment capacities and improved the deformation and failure responses, particularly at high eccentricity. Therefore, SC-RPC shells can substantially enhance the structural performance and safety of slender hybrid reinforced concrete columns subjected to biaxial eccentric loading.

ARTICLE INFO

Article history:
Received – November 25, 2025
Revision requested – January 16, 2026
Revision received – February 16, 2026
Accepted – February 25, 2026

Keywords:
Reactive powder concrete
Self-compacting concrete
Biaxial loading
Hybrid concrete columns
Slender columns

This is an open access article distributed under the CC BY licence.
© 2026 by the Authors.

Citation: Al-Taai AAS, Waryosh WA (2026). Structural performance of biaxially-loaded slender hybrid self-compacting concrete columns with RPC shells. *Challenge Journal of Concrete Research Letters*, 17(2), 109–121.

1. Introduction

From a structural perspective, reinforced concrete columns are generally classified as short or slender members. Slender columns are increasingly used in modern construction, including tall buildings, large-span arenas, shopping centers, and multilevel parking facilities. However, their high slenderness ratios amplify second-order effects and lateral deflections under combined axial compression and bending, which may compromise structural safety and serviceability (Al-Taai et al. 2018; ACI 318M-19 2019; Al-Taai 2025). Accordingly, understanding the response of slender columns under combined loading is essential for the development of safer and more efficient structural systems.

To overcome the limitations of conventional slender columns, researchers have investigated composite and hybrid reinforced concrete systems in which the interaction between different materials can improve structural efficiency and economy. Experimental studies on concrete-filled steel members have shown that effective composite interaction can increase load-carrying capacity and delay local instability (Sancıoğlu et al. 2025). At the structural-system level, steel-concrete composite columns have also been reported to increase lateral rigidity and reduce storey displacements relative to conventional reinforced concrete columns (Yıldız and Şermet 2025). Composite columns containing steel I-sections encased in concrete have been widely investigated (Begum et al. 2013; Lai et al. 2019a, 2019b; Xie et al. 2019; Mao et al. 2021; Chen et al. 2022; Yuan et al. 2022; Hu et al. 2023; Liu et al. 2023). Concrete-filled steel and aluminum tubes have likewise been studied extensively, while external CFRP confinement has been used to im-

* *Corresponding author*. E-mail address: alaaalisalman@uomustansiriyah.edu.iq (A. A. S. Al-Taai)
ISSN: 2548-0928 / DOI: https://doi.org/10.20528/cjcrl.2026.02.003

prove the strength and ductility of short square columns (Wang et al. 2019; Patel et al. 2020; Deng et al. 2021; Bu et al. 2023; Rong 2023; Xu et al. 2024).

A hybrid concrete column combines two concrete types within a common cross-section, typically a high-strength outer shell and a normal-strength core (Resheq 2018; Al-Zuhairi 2021). The high-strength shell can contribute substantially to load resistance while also protecting the core against environmental and thermal effects. Because the structural response depends on the integrity of the outer layer, cracking or damage to the shell may adversely affect the performance of the entire cross-section (Richart and Brown 1934).

In hybrid concrete columns, the two concrete layers may act together through either full or partial interfacial bond. Several studies have examined the effect of this interaction on the behavior of short hybrid columns (Ali and Mohammed 2018; Mohammed Ali 2020). Ali and Mohammed (2018) investigated eccentrically loaded columns composed of a precast RPC shell and a normal-strength concrete core. Increasing the shell thickness from 25 to 50 mm increased the load capacity by approximately 11%, while the combined use of longitudinal and transverse reinforcement enhanced ductility compared with unreinforced specimens.

Mohammed Ali (2020) evaluated the concentric and eccentric performance of hybrid columns comprising a high-strength RPC shell and a low-strength concrete core bonded with epoxy resin. Under concentric loading, the ultimate capacity increased by 28-80%, depending on the shell strength, while the eccentrically loaded columns also exhibited stable and satisfactory behavior.

Several studies have investigated short hybrid columns designed with full bond between the outer and inner concrete layers (Latief 2018; Resheq 2018; Hamid et al. 2020; Mohammed et al. 2022; Mufja 2024). These studies have improved understanding of how full composite interaction affects cross-sectional response and overall load-carrying capacity.

Latief (2018) studied hybrid columns composed of high-strength concrete (HSC) and steel fiber-reinforced concrete (SFRC) and reported that both the outer-shell material and the eccentricity ratio (e/h) strongly affected the structural response. For eccentricity ratios of 1/3 and 1/2, the ultimate capacities of columns with HSC shells increased by 3.74% and 21.08%, respectively, while those of columns with SFRC shells increased by 3.74% and 11.11%, respectively. Resheq (2018) examined the effects of concrete type and sectional configuration on axial capacity. The load capacity increased by 70% when the diameter of the normal-concrete core was reduced and that of the SCC shell was increased, whereas the reverse configuration produced an increase of 20%. Al-Zuhairi (2021) investigated the axial capacity of short hybrid columns under biaxial loading and reported a 33.5% increase relative to conventional columns. The capacity increased by 38% when the hybrid ratio decreased from 0.36 to 0.16, and the lower hybrid ratio also reduced the axial strain at a given load level.

Hamid et al. (2020) assessed the influence of reinforcement detailing on short hybrid columns comprising a normal-concrete core and a 40 mm thick RPC outer shell. The combined use of the two concretes increased the ultimate load by 179% relative to the conventional concrete specimens, and transverse reinforcement had a greater influence on the response than longitudinal reinforcement. Mohammed et al. (2022) subsequently examined the effects of transverse-bar diameter and spacing in columns with the same 40 mm RPC shell. Increasing the bar diameter produced the greatest strength improvement, with an increase of 203% in ultimate load, while reducing the spacing increased the load by approximately 179% relative to the reference specimen. Mufja (2024) investigated the effects of eccentricity and outer-shell thicknesses of 25 and 50 mm in hybrid columns with a high-strength concrete core and an RPC shell. Three RPC mixtures were examined: 1% steel fiber (SF), 0.5% SF plus 0.5% polypropylene fiber (PPF), and 1% PPF. The mixture containing 1% SF exhibited the greatest axial stiffness and energy absorption. The ultimate loads increased by 12-28% for square sections and 26-35% for circular sections relative to the reference specimens. Overall, previous studies indicate two principal fabrication strategies: using a normal- or low-strength core confined by a high-strength or fiber-reinforced shell, and combining two concretes with markedly different mechanical properties. Because numerical predictions of reinforced concrete strength can vary with the adopted constitutive model, experimental studies remain essential for reliable characterization of hybrid systems (Polat and Karaman 2025).

The authors' previous studies provided detailed experimental assessments of slender hybrid SCC columns with normal-concrete cores and RPC outer shells under uniaxial eccentric loading (Al-Taai and Waryosh 2025, 2026). In the uniaxial loading study, replacing the outer shell with RPC increased the axial load capacity by 57.8% and the flexural moment capacity by 56%, while improving energy dissipation and reducing lateral deformation (Al-Taai and Waryosh 2026). In the related strengthening study, the hybrid columns were externally strengthened using near-surface-mounted (NSM) GFRP bars in combination with CFRP sheets. The strengthened specimens achieved approximately 80% greater axial load capacity and more than a 100% increase in flexural moment capacity relative to the unstrengthened specimens (Al-Taai and Waryosh 2025). These findings demonstrate the effectiveness of RPC shells and NSM strengthening in improving the strength, ductility, and overall response of slender SCC columns under eccentric compression.

The use of two concretes within a single hybrid cross-section requires both mixtures to possess sufficient flowability and cohesion so that the outer shell can fully encapsulate the inner core and develop a continuous interface without segregation or weak zones (Hassan 2015; Danha et al. 2020; Hussein et al. 2020; Al-Taai et al. 2025). Consequently, using two self-compacting concretes is a practical fabrication approach. Nevertheless, hybrid sections formed entirely from self-compacting concretes, particularly those incorporating RPC as an outer shell, have not been examined in sufficient detail. Research on slender hybrid SCC columns under biaxial eccentric loading is also scarce. The present study therefore experimentally investigates the structural performance of slender hybrid SCC columns subjected to biaxial eccentric compression, with full bond between the core and outer shell.

2. Experimental Details

2.1. Specimen description

Six slender reinforced concrete columns were prepared, each with a square cross-section of 140 × 140 mm and an overall height of 1260 mm, corresponding to a slenderness ratio of approximately 30. The longitudinal reinforcement comprised four 10 mm diameter deformed bars, providing a reinforcement ratio (ρ) of 1.6%, with a concrete cover of 22.5 mm. The detailing satisfied the minimum column reinforcement requirements of ACI 318-19 (ACI 318M-19 2019). The longitudinal bars had a yield strength of 630 MPa and an elastic modulus of 200 GPa. Closed 6 mm diameter stirrups spaced at 140 mm along the column height were used as transverse reinforcement. The column geometry and reinforcement layout are shown in Fig. 1. Two corbels were cast at the ends of each column to introduce biaxial eccentricity. The corbels were designed to resist the full test load and ensure that failure occurred within the intended test region. Each corbel had plan dimensions of 260 × 260 mm and a depth of 280 mm.

A loading system was specifically designed to apply biaxially eccentric compression to the slender columns and to promote failure within the central test region rather than near the ends. Each specimen was positioned near one corner of the corbels to provide the required offsets for the eccentric load. The load was applied horizontally in a biaxial configuration.

2.2. Test matrix

The experimental program comprised the six slender column specimens summarized in Table 1. All specimens had identical geometric and reinforcement details, while the investigated variables were the outer-shell concrete type and the biaxial eccentricity level. Three eccentricity ratios were considered: low (e_x/b_x=e_y/b_y=0.25), medium (e_x/b_x=e_y/b_y=0.65), and high (e_x/b_x=e_y/b_y= 0.90), corresponding to Groups 1, 2, and 3, respectively. Here, e_x and e_y denote the load eccentricities about the two principal axes, while b_x and b_y are the corresponding section dimensions. Each group included one reference column cast entirely with SC-NC and one hybrid column composed of an SC-NC core and an SC-RPC outer shell. The reference specimens were designated NBE1, NBE2, and NBE3, whereas the hybrid specimens were designated RBE1, RBE2, and RBE3.

The experimental program was designed to determine how biaxial eccentricity influences the load capacity, stiffness, and deformation response of slender hybrid columns and to evaluate the contribution of the RPC shell as a confining and load-resisting layer. The selected eccentricity ratios represent compression-controlled, near-balanced, and tension-controlled response conditions.

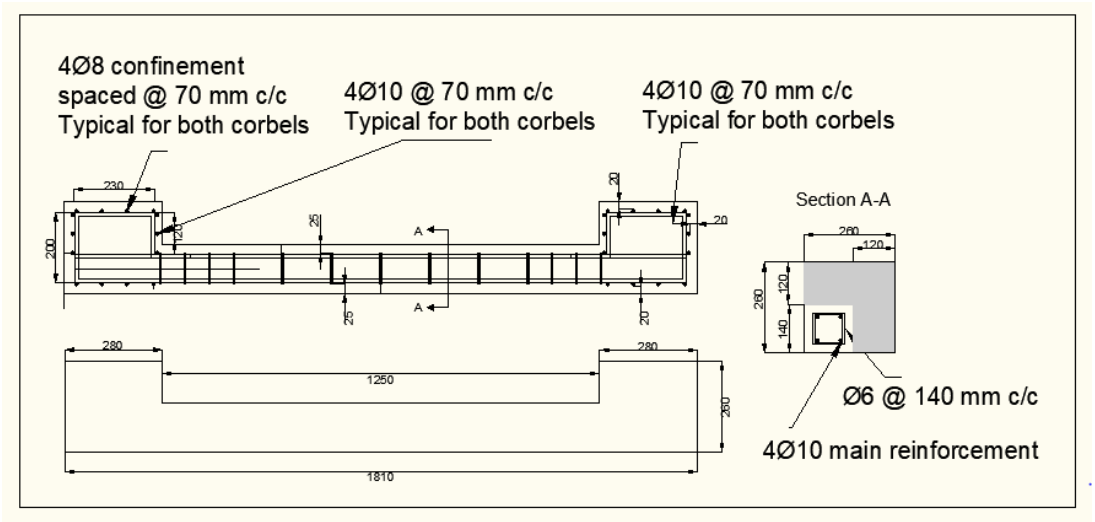

Fig. 1. Reinforcement layout of the hybrid SCC columns.

Table 1. Test matrix for biaxial loading.

Group	Eccentricity ratio	Self-compacting hybrid concrete (SC-HC)				Specimen designation
		Outer-shell concrete		Inner-core concrete		
		Concrete type	Grade (MPa)	Concrete type	Grade (MPa)	
1	e_x/b_x = 0.25	SC-NC	33.79	SC-NC	33.79	NBE1
		SC-RPC	100.16			RBE1
2	e_x/b_x = 0.65	SC-NC	33.79			NBE2
		SC-RPC	100.16			RBE2
3	e_x/b_x = 0.9	SC-NC	33.79			NBE3
		SC-RPC	100.16			RBE3

2.3. Specimen instrumentation

The biaxial loading tests were conducted using a servo-controlled testing machine with a maximum capacity of 3000 kN. Each specimen was subjected to monotonically increasing static load until failure. The instrumentation arrangement is shown in Fig. 2. Three linear variable differential transformers (LVDTs) were positioned at the lower, middle, and upper levels of each specimen to measure lateral displacement. Two strain gauges were installed on the longitudinal reinforcement at mid-height: SG1 on the tension side of the loaded axis and SG2 on the compression side of the opposite axis. The load was applied in 10 kN increments until failure. Load, strain, and displacement data were recorded automatically using a computer-based data acquisition system.

2.4. Test setup and procedure

The compressive load was applied using a hydraulic jack positioned between two steel loading caps. Each cap consisted of a 270 × 270 × 40 mm steel plate and four 270 × 150 × 10 mm side plates, which ensured uniform load distribution and reduced local stress concentrations. A semicircular knife edge was attached to the loading assembly, and the upper cap contained grooves aligned with the calculated eccentricity directions about the principal axes. This arrangement transferred the biaxially eccentric load through the knife-edge lines. A hinge connection permitted free rotation and prevented the development of unintended end moments. The loading caps, hinge arrangement, and complete test setup are shown in Fig. 3.

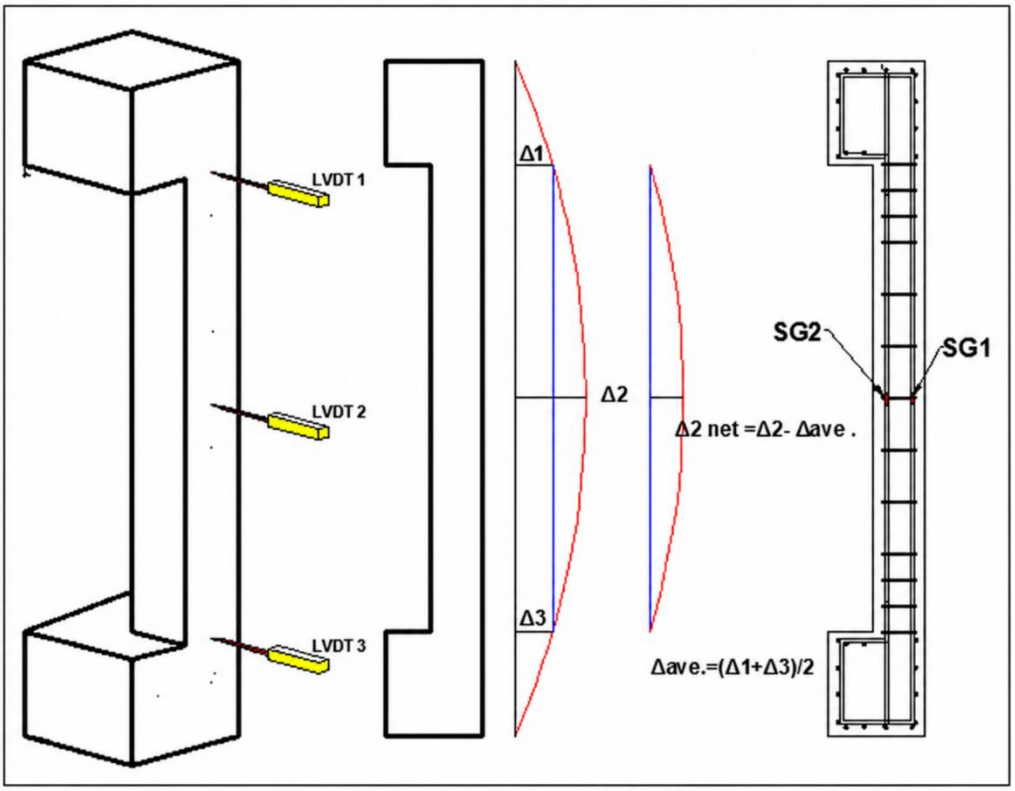

Fig. 2. Layout of the LVDTs and strain gauges installed on the longitudinal bars.

2.5. Materials

A series of trial mixtures was prepared to determine suitable self-compacting concrete compositions for the present study. The selected mixtures were required to possess adequate filling ability, passing ability, and resistance to segregation so that they could flow and consolidate under their own weight while producing uniform specimens.

The trial program produced the mixtures listed in Table 2. The specimens examined in the present study were cast using SC-NC and SC-RPC, with target compressive strengths of approximately 30 and 90 MPa, respectively.

All concrete mixtures were produced using ordinary Portland cement complying with Iraqi Specification No. 5 (IQS No. 5 2019). Crushed natural stone with a nominal maximum size of 10 mm and a sulfate content of 0.06% was used as the coarse aggregate, while crushed-stone sand with a sulfate content of 0.12% was used as the fine aggregate. Silica fume containing approximately 92% SiO_2 was incorporated to improve strength and durability. Previous experimental findings have shown that silica fume improves the mechanical performance of RPC by enhancing particle packing and promoting additional C-S-H formation, thereby producing a denser and less porous matrix (Shaheen et al. 2025). Straight steel fibers with a length of 13 mm, a diameter of 0.2 mm, and a tensile strength of 2500 MPa were used, corresponding to an aspect ratio of 65.

A high-performance superplasticizer (MasterGlenium 54) based on modified polycarboxylic ether chemistry was used in all SCC mixtures to achieve the required workability without compromising strength. The admixture, supplied by MBCC Group, was light brown, had a

specific gravity of approximately 1.07 and a pH of 5-8, and complied with ASTM C494 Types F and G (ASTM C494/C494M-19 2019).

The adopted dosage produced a slump flow greater than 600 mm and satisfied the EFNARC (2002) criteria for self-compacting concrete.

At 28 days, the measured compressive strengths were 33.79 MPa for Mix 1 and 88.86 MPa for Mix 2.

Deformed bars with a diameter of 10 mm (Grade 520) and a measured yield strength of 630 MPa were used as longitudinal reinforcement, while 6 mm diameter plain bars of the same grade were used as transverse reinforcement. The measured mechanical properties of the reinforcement are summarized in Table 3.

2.6. Casting and preparation of the test columns

Each specimen was cast vertically to maintain uniform placement and proper integration of the concrete layers. For the hybrid columns, an aluminum tube measuring 100 × 100 × 1.5 mm was installed within the steel mold to separate the inner core from the outer shell during casting. The tube was secured at its upper edges to prevent movement during placement and to facilitate removal after both concretes had been poured.

The reference reinforced concrete columns were cast in a single pour without an internal separator. In the hybrid specimens, the core and shell concretes were placed successively under fresh-to-fresh conditions to ensure full bond and composite interaction. Fig. 4 presents the cross-sectional configurations, and Fig. 5 shows the principal fabrication stages.

Fig. 3. Test setup and loading configuration.

Table 2. Mixture proportions of the self-compacting concretes.

Mixture	Cement (kg/m^3)	Sand (kg/m^3)	Gravel (kg/m^3)	Water (kg/m^3)	MasterGlenium 54 (kg/m^3)	Water/binder ratio	Silica fume (kg/m^3)	Steel fiber (kg/m^3)	28-day compressive strength (MPa)
SC-NC	360	780	830	158.50	6.40	0.440	–	–	33.79
SC-HSC	500	840	871	167.50	10.45	0.304	50	–	55.22
SC-RPC	950	1050	–	209.76	45.60	0.184	190	78.5	88.86

Table 3. Mechanical properties of the reinforcement.

Reinforcement diameter	Yield strength (MPa)	Ultimate strength (MPa)	Elongation (%)
6 mm	526	580	13.9
8 mm	354	561	24.1
10 mm	630	691	9.8

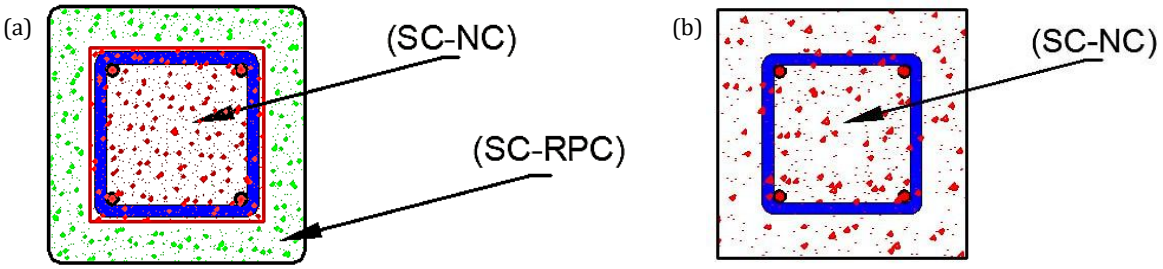

Fig. 4. Cross-sectional details of (a) hybrid self-compacting concrete columns and (b) normal self-compacting concrete columns.

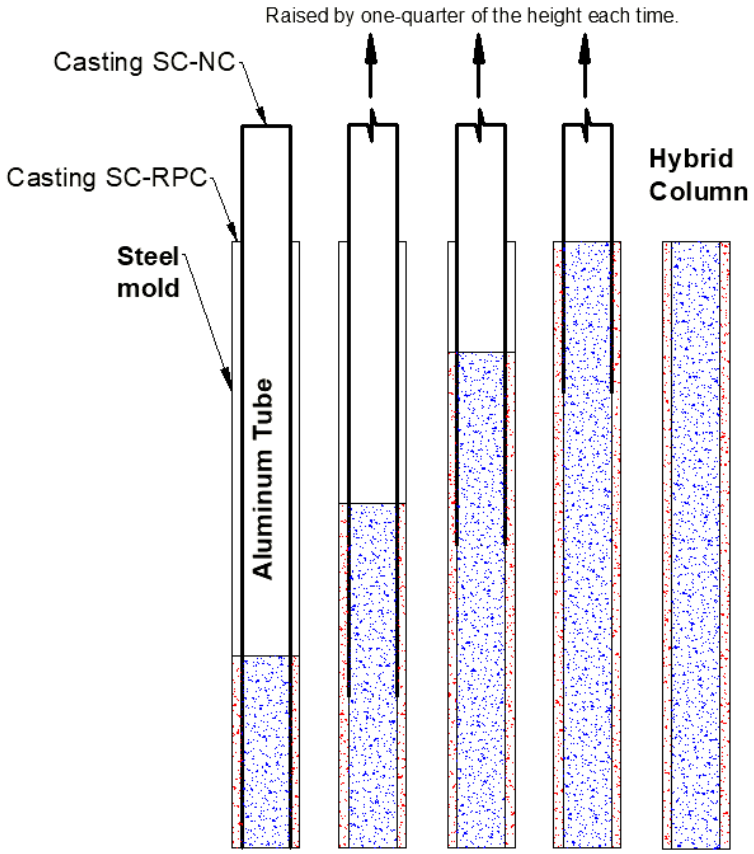

Fig. 5. Main stages of hybrid column fabrication.

3. Experimental Results

3.1. Load-lateral deflection relationships

Figs. 6–8 show the load-lateral deflection responses of the columns at eccentricity ratios of 0.25, 0.65, and 0.90, respectively. The results demonstrate that the outer-shell strength significantly influenced the lateral response of the hybrid columns under biaxial eccentric loading.

The outer layer was varied between SC-NC and SC-RPC to assess the effect of material strength. Lateral displacement was measured using three LVDTs positioned near the two ends and at mid-height, and the mid-height response was used for the load-deflection curves. The response of each specimen was approximately linear at the initial loading stage, followed by a reduction in stiffness and a rapid increase in lateral deflection near the ultimate load. The post-peak branches showed decreasing load with continued deformation. Table 4 summarizes the ultimate loads and corresponding lateral deflections. Relative to the reference specimens, the use of an SC-RPC shell increased the ultimate load by 45.96% for RBE1 (e_x/b_x=0.25), 59.67% for RBE2 (e_x/b_x=0.65), and 80.53% for RBE3 (e_x/b_x=0.90). This behavior is attributed to the higher compressive strength and elastic modulus of RPC, which increase the flexural stiffness of the section, delay cracking and stiffness degradation, and improve load-carrying capacity, particularly at high eccentricity where bending effects dominate.

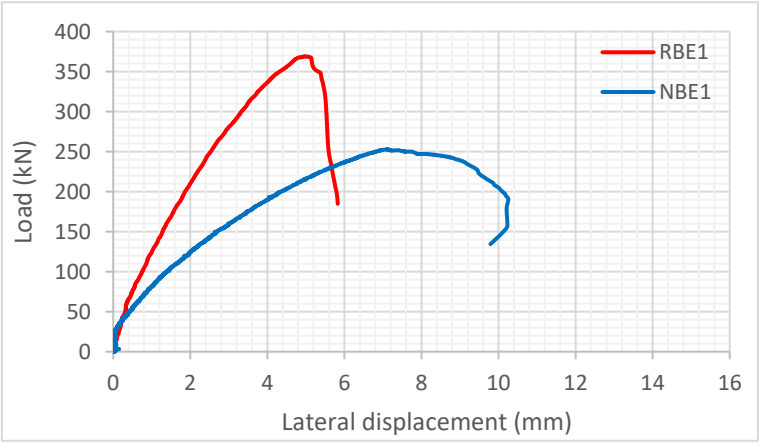

Fig. 6. Load-lateral deflection relationship at the low eccentricity ratio.

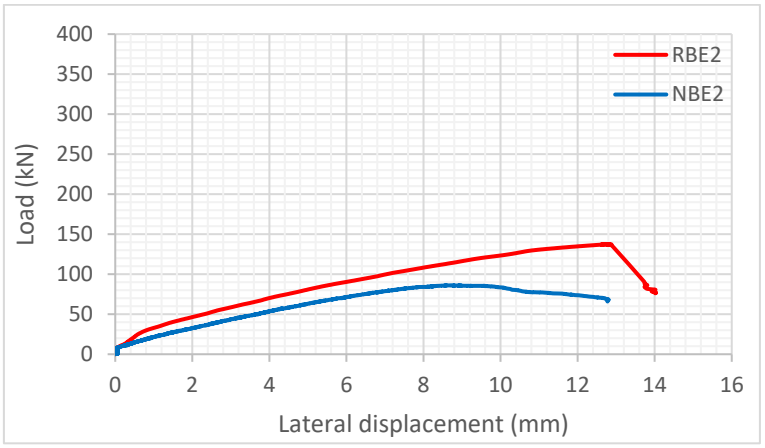

Fig. 7. Load-lateral deflection relationship at the medium eccentricity ratio.

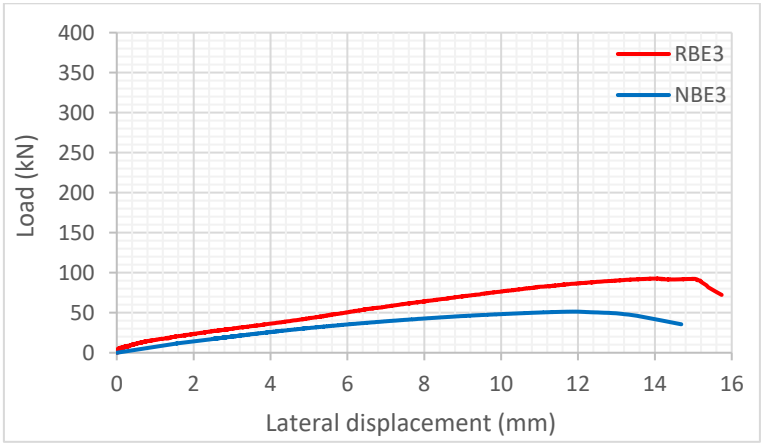

Fig. 8. Load-lateral deflection relationship at the high eccentricity ratio.

Table 4. Ultimate loads and lateral displacements of the biaxially loaded specimens.

No.	Specimen	P_u (kN)	Lateral deflection, Δ_u (mm)	Increase in P_u (%)
1	NBE1	252.86	7.116	0
2	RBE1	369.08	4.973	45.964
3	NBE2	86.034	8.699	0
4	RBE2	137.37	12.79	59.671
5	NBE3	51.348	11.92	0
6	RBE3	92.701	14.07	80.534

3.2. Load-longitudinal steel strain relationships

Figs. 9–11 illustrate the longitudinal steel strain responses at the mid-height of the specimens. In all biaxially loaded columns, the tensile reinforcement reached its yield strain before failure. At the low eccentricity ratio (e_x/b_x=0.25), yielding occurred at approximately 92% and 97% of the ultimate load for NBE1 and RBE1, respectively. At the medium eccentricity ratio (e_x/b_x=0.65), yielding occurred at 87% and 88% of the ultimate load for NBE2 and RBE2, respectively, accompanied by greater sectional rotation and lateral deflection. At the high eccentricity ratio (e_x/b_x=0.90), yielding occurred at 81% and 76% of the ultimate load for NBE3 and RBE3, respectively, with larger curvature and deformation beyond the balanced condition.

The compression reinforcement did not reach yield in any specimen, confirming that the response was governed primarily by tension-controlled behavior. The columns therefore exhibited ductile characteristics influenced by the applied eccentricity and the location of the outermost tensile reinforcement. Consequently, the tension bars yielded before significant compression failure developed in the concrete.

As the eccentricity increased, the bending moment, curvature, and tensile strains in the longitudinal reinforcement also increased. The neutral axis shifted toward the compression face, causing the tensile reinforce-

ment to yield at a smaller proportion of the ultimate load. This trend is consistent with the expected response of eccentrically loaded slender columns, in which flexural effects become increasingly dominant.

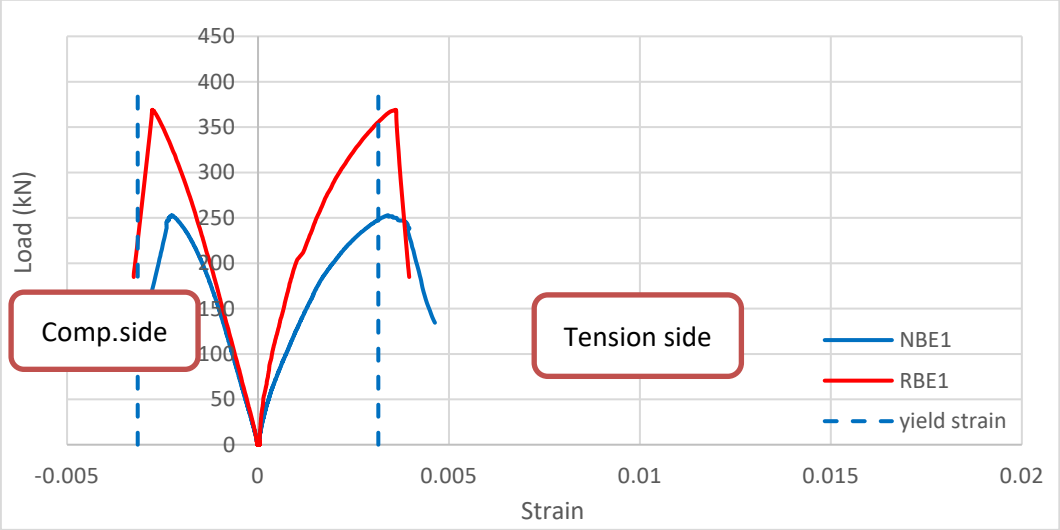

Fig. 9. Load-longitudinal steel strain relationship at the low eccentricity ratio.

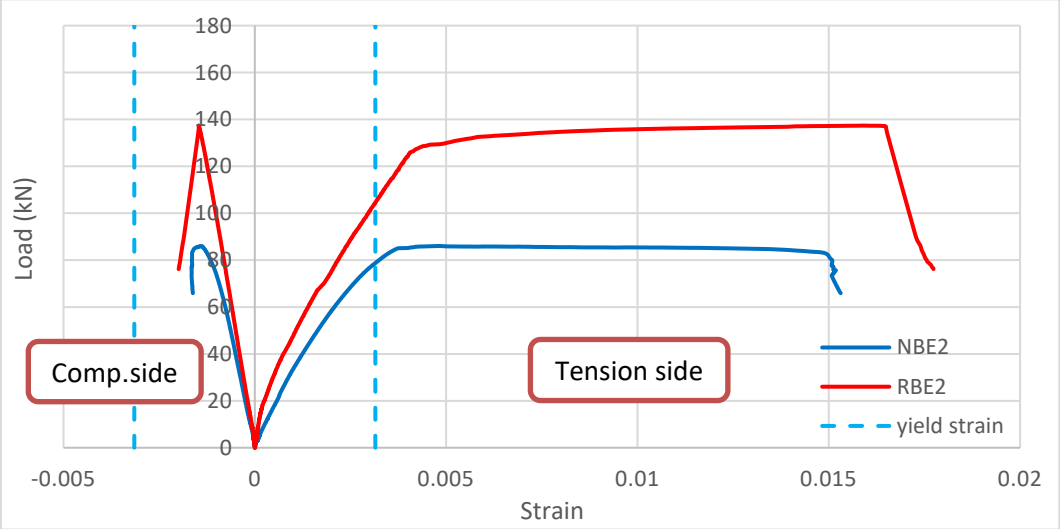

Fig. 10. Load-longitudinal steel strain relationship at the medium eccentricity ratio.

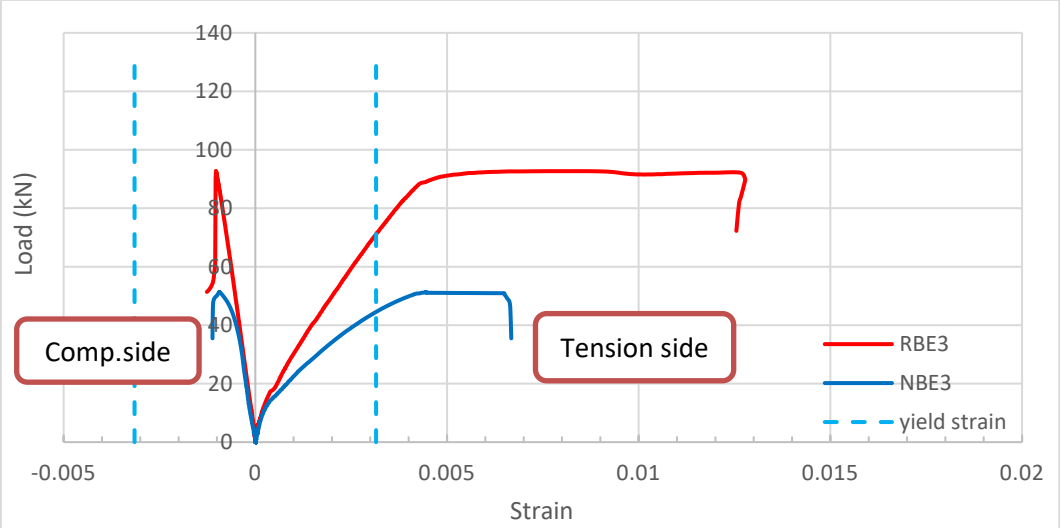

Fig. 11. Load-longitudinal steel strain relationship at the high eccentricity ratio.

3.3. Moment-curvature response

All specimens were subjected to eccentric compressive loading, resulting in biaxial bending about the principal axes. The moment-curvature relationships for the three experimental groups are shown in Figs. 12–14. At each load increment, the bending moment (M) was calculated as the product of the applied load (P) and the effective eccentricity, defined as the sum of the initial eccentricity (e) and the lateral deflection (Δ) measured at mid-height, as expressed in Eq. (1):

$$M_u = P(e + \Delta) \quad (1)$$

Curvature varied across the section during testing. It was evaluated using the plane-sections assumption, under which the longitudinal strain distribution is linear through the section depth. The curvature was therefore calculated using Eq. (2):

$$\phi_i = \frac{\varepsilon_{sti} - \varepsilon_{sci}}{d} \quad (2)$$

where ε_{sti} and ε_{sci} denote the measured strains in the tensile and compressive longitudinal reinforcement, respectively, and d is the distance between the two reinforcement layers. This distance remained constant at 289 mm for all tested columns. Table 5 summarizes the ultimate axial load, the corresponding lateral displacement, and the ultimate bending moment calculated as $M_u = P_u\ (e + \Delta_u)$. Replacing the SC-NC shell with SC-RPC increased the ultimate moment by 38.54% for RBE1, 66.64% for RBE2, and 83.47% for RBE3 relative to the corresponding reference specimens. The higher compressive strength and elastic modulus of RPC increased the flexural stiffness of the section, delayed cracking and stiffness degradation, and enabled the columns to sustain greater moments and curvatures before failure. This effect became more pronounced at higher eccentricity ratios, where flexural action governed the response.

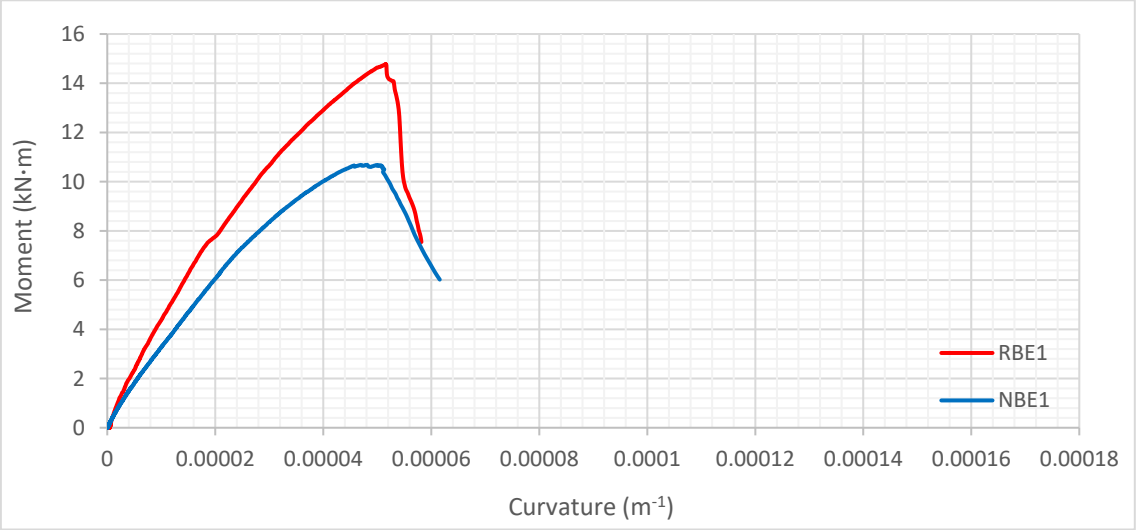

Fig. 12. Moment-curvature relationship at the low eccentricity ratio.

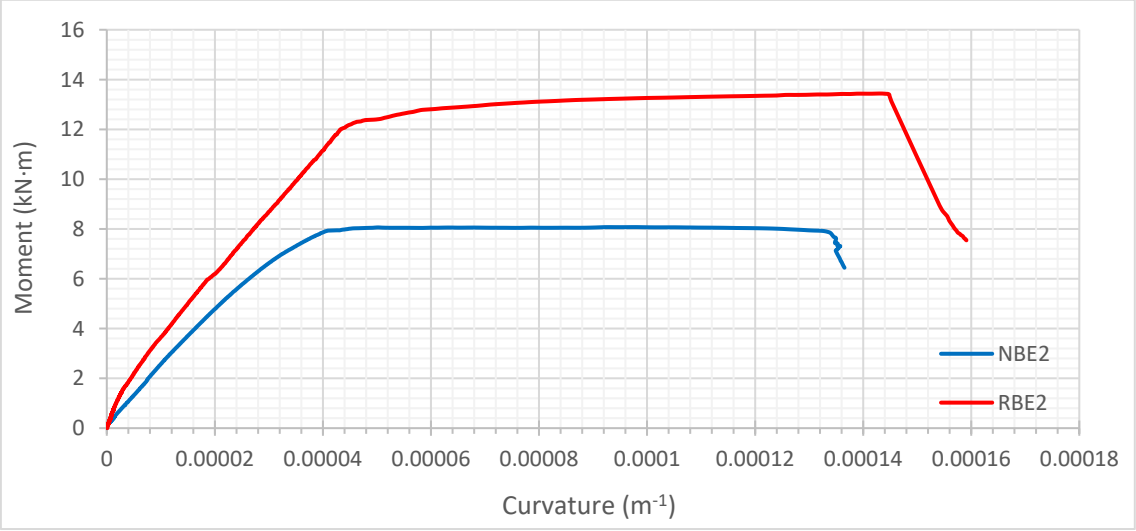

Fig. 13. Moment-curvature relationship at the medium eccentricity ratio.

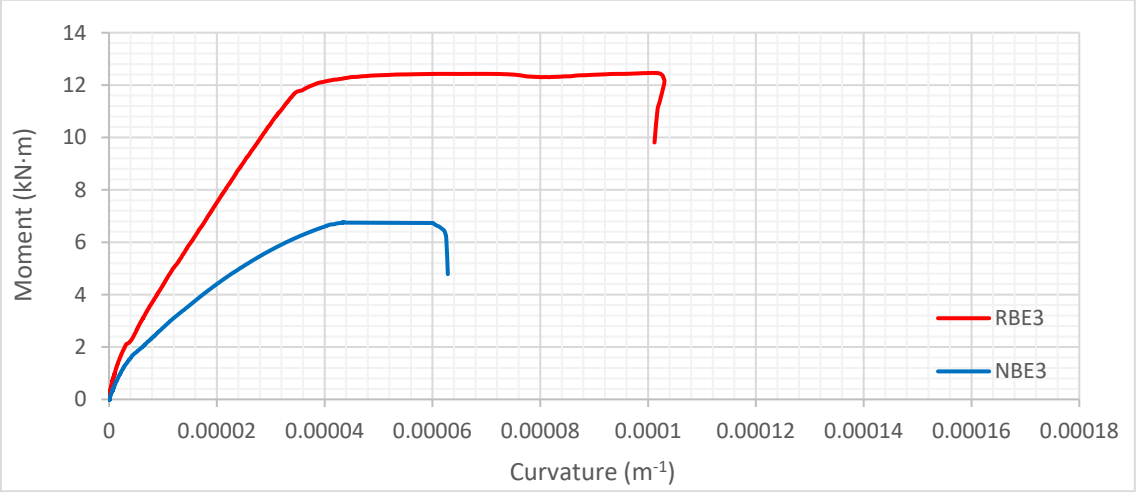

Fig. 14. Moment-curvature relationship at the high eccentricity ratio.

Table 5. Ultimate moment-curvature results for the biaxially loaded specimens.

No.	Specimen	P_u (kN)	Δ_u (mm)	$M_u = P_u\,(e + \Delta_u)$ (kN·m)	Curvature (1/mm)	Increase in M_u (%)
1	NBE1	252.86	7.116	10.649	4.56E-05	0
2	RBE1	369.08	4.973	14.753	5.14E-05	38.538
3	NBE2	86.034	8.699	8.061	5.02E-05	0
4	RBE2	137.37	12.79	13.433	1.40E-04	66.641
5	NBE3	51.348	11.92	6.774	4.35E-05	0
6	RBE3	92.701	14.07	12.428	6.15E-05	83.466

3.4. Curvature ductility, flexural stiffness, and energy absorption

Flexural stiffness is a key parameter governing the resistance of a column to lateral deformation and second-order effects. The effective flexural stiffness (EI_{eff}) of each tested column was derived from its moment-curvature response using the procedure described below:

$$EI_{eff} = \frac{M_{ty}}{\phi_y} \quad (3)$$

$$\mu_\phi = \frac{\phi_u}{\phi_y} \quad (4)$$

Fig. 15 schematically illustrates the procedure used to determine the yield curvature, ultimate curvature, and curvature ductility ratio. In this analysis, EI_{eff} denotes the effective flexural stiffness, and M_{ty} is the moment corresponding to initial yielding of the longitudinal reinforcement. The parameters ϕ_y and ϕ_u represent the curvatures at yielding and at 80% of the post-peak moment, respectively. To estimate ϕ_y, a line was drawn from the origin of the M-ϕ curve to the point corresponding to $0.75M_u$. The intersection of this line with the tangent at the ultimate moment was taken as the yield curvature, following the procedure proposed by El-Tawil and Deierlein (1999).

The comparisons in Table 6 show that the effect of the RPC shell on curvature ductility depended on the eccentricity level. At low eccentricity, the ductility ratio decreased slightly from 1.333 for NBE1 to 1.313 for RBE1. At medium eccentricity, it increased from 2.594 to 3.125, while at high eccentricity it increased markedly from 1.37 to 2.94. The hybrid specimens also exhibited greater flexural stiffness than the corresponding reference columns at all three eccentricity levels, indicating that the RPC shell improved deformation control under biaxial bending. Energy absorption increased from 1.725 to 1.771 at low eccentricity, from 2.389 to 3.769 at medium eccentricity, and from 1.803 to 4.094 at high eccentricity. Thus, the RPC outer shell consistently improved stiffness and energy absorption, while its influence on ductility became more beneficial as the eccentricity increased.

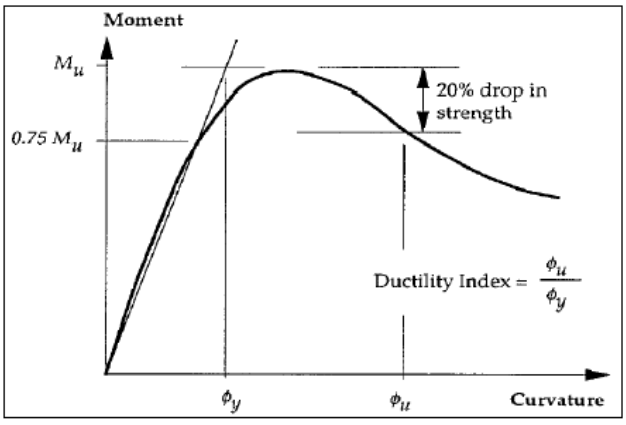

Fig. 15. Definition of the curvature ductility ratio according to El-Tawil and Deierlein (1999).

Table 6. Flexural stiffness, curvature ductility, and energy absorption of the biaxially loaded specimens.

No.	Specimen	M_u (kN·m)	ϕ_u (1/mm)	ϕ at $0.80M_u$ (1/mm)	ϕ at $0.75M_u$ (1/mm)	Curvature ductility	Flexural stiffness (kN·mm^2)	Energy absorption
1	NBE1	10.649	4.56E-05	0.000056	0.000042	1.333	373.710	1.725
2	RBE1	14.753	5.14E-05	0.000055	0.000042	1.313	478.553	1.771
3	NBE2	8.061	5.02E-05	0.000093	0.000036	2.594	396.060	2.389
4	RBE2	13.433	1.40E-04	0.000015	0.000048	3.125	415.215	3.769
5	NBE3	6.774	4.35E-05	0.000046	0.000034	1.370	246.619	1.803
6	RBE3	12.428	6.15E-05	0.000010	0.000034	2.940	303.819	4.094

Table 7. Observed failure modes of the tested specimens.

No.	Specimen	Failure mode	Description
1	NBE1	Compression failure	Sudden concrete crushing between the upper and middle thirds of the column, with visible cracking on the opposite tension face.
2	RBE1	Compression failure	Sudden concrete crushing in the upper third of the column, with visible cracking on the opposite tension face.
3	NBE2	Flexural failure	A wide crack developed in the middle third of the tension zone, accompanied by crushing in the middle third of the compression zone.
4	RBE2	Flexural failure	Cracks developed along the column, including a wide crack between the upper and middle thirds.
5	NBE3	Flexural-compression failure	Visible cracks developed on the tension side and widened with increasing load, while slow, localized concrete crushing occurred near mid-height on the opposite face.
6	RBE3	Flexural failure	A wide crack developed in the lower third of the tension zone, accompanied by slight crushing on the opposite face.

Fig. 16. Observed failure modes of the tested specimens.

4. Conclusions

- Replacing the SC-NC outer shell with SC-RPC substantially increased the ultimate load capacity of the hybrid columns under biaxial eccentric loading. The increases were 45.96%, 59.67%, and 80.53% at low, medium, and high eccentricity, respectively, indicating that the contribution of the RPC shell became more pronounced as the eccentricity increased.
- All specimens exhibited nonlinear load-deflection behavior. The RPC-shell columns sustained higher peak loads and generally maintained greater stiffness, demonstrating improved resistance to deformation and delayed stiffness degradation.
- The RPC-shell columns exhibited enhanced post-peak deformation capacity and energy absorption relative to the reference specimens, particularly at medium and high eccentricity. These results show that RPC improved not only strength but also the ability of the columns to sustain deformation before failure.
- The SC-RPC outer shell increased the ultimate flexural moment capacity by 38.54%, 66.64%, and 83.47% at low, medium, and high eccentricity, respectively, relative to the corresponding reference specimens.
- The influence of the RPC shell on curvature ductility depended on eccentricity. A slight reduction was observed at low eccentricity, whereas substantial improvements occurred at medium and high eccentricity.
- Although stiffness decreased as eccentricity increased, the hybrid columns retained greater stiffness and absorbed more energy than the corresponding reference columns. This response suggests that RPC shells may be beneficial in applications involving severe deformation demands, although dedicated cyclic or dynamic tests are required to confirm their seismic performance.
- The columns failed in compression, flexure, or combined flexural-compression modes, depending on eccentricity. The hybrid specimens generally exhibited more distributed cracking and less abrupt localized crushing, providing a more gradual failure response and an improved safety margin.

Acknowledgements

None declared.

Funding

The authors received no financial support for the research, authorship, and/or publication of this manuscript.

Conflict of Interest

The authors declare no potential conflicts of interest with respect to the research, authorship, and/or publication of this manuscript.

Data Availability

The datasets generated and/or analyzed during the current study are not publicly available but are available from the corresponding author upon reasonable request.

AI Assistance

No AI-based tools were used in the preparation of this manuscript.

Author Contributions

All authors made substantial contributions to the conception and design of the study, acquisition of data, analysis and interpretation of data; drafted or critically revised the manuscript for important intellectual content; and approved the final version to be published.

REFERENCES

ACI 318M-19 (2019). Building code requirements for structural concrete and commentary. American Concrete Institute, Farmington Hills, MI, USA.

Ali A, Mohammed Z (2018). Strength evaluation of hybrid reinforced concrete columns under eccentric loads. *Engineering and Technology Journal*, 36(4A), 449-455.

Al-Taai AAS (2025). Finite element analysis of concrete filled circular steel tube short columns subjected to axial compression load. *Mathematical Modelling of Engineering Problems*, 12(5), 1687-1694.

Al-Taai AAS, Al-Ibadi AHD, Al-Bayati JK (2025). Behavior of fibrous concrete slabs under static and impact loads. *Mathematical Modelling of Engineering Problems*, 12(6), 2148-2156.

Al-Taai AAS, Hassan SA, Hussein LF (2018). Finite element analysis of corner strengthening of CFRP-confined concrete column. *IOP Conference Series: Materials Science and Engineering*, 454(1), 012088.

Al-Taai AAS, Waryosh WA (2025). Structural behavior of slender hybrid self-compacting concrete columns with RPC shells and NSM technique. *Journal of Building Pathology and Rehabilitation*, 11(1), 42.

Al-Taai AAS, Waryosh WA (2026). Influence of load eccentricity on structural response of slender hybrid self-compacting concrete columns with reactive powder concrete shells under uniaxial loading. *International Journal of Engineering*, 39(8), 2022-2034.

Al-Zuhairi AH (2021). Structural behavior of reinforced hybrid concrete columns under biaxial loading. *Latin American Journal of Solids and Structures*, 18(6), 1-18.

ASTM C494/C494M-19 (2019). Standard specification for chemical admixtures for concrete. ASTM International, West Conshohocken, PA, USA.

Begum M, Driver RG, Elwi AE (2013). Behaviour of partially encased composite columns with high strength concrete. *Engineering Structures*, 56, 1718-1727.

Bu J, Liu Q, Yu Y, Qiu Q (2023). Axial compression performance and bearing capacity calculation of round-ended concrete-filled aluminum tube column. *Applied Sciences*, 13(13), 7918.

Chen Z, Ning F, Song C, Liang Y (2022). Study on axial compression bearing capacity of novel concrete-filled square steel tube columns. *Journal of Building Engineering*, 51, 104298.

Danha LS, Abdul-Hussien ZA, Abduljabbar MS, Yassin LAG (2020). Flexural behavior of hybrid ultra-high-performance concrete. *IOP Conference Series: Materials Science and Engineering*, 737(1), 012008.

Deng ZH, Guo JH, Yu JJ, Liu B (2021). Axial compression performance of coral concrete-filled aluminium tube (CCFAT) square stub columns. *Case Studies in Construction Materials*, 15, e00697.

EFNARC (2002). Specifications and guidelines for self-compacting concrete. European Federation for Specialist Construction Chemicals and Concrete Systems, Warrington, UK.

El-Tawil S, Deierlein GG (1999). Strength and ductility of concrete encased composite columns. *Journal of Structural Engineering*, 125(9), 1009-1019.

Hamid MM, Yassin LAG, Mohammed AH (2020). Behavior of hybrid reinforced concrete columns. *IOP Conference Series: Materials Science and Engineering*, 737(1), 012033.

Hassan FH (2015). Behavior of hybrid deep beams containing ultra high performance and conventional concretes. *Engineering and Technology Journal*, 33(1A), 30-50.

Hu HS, Yang ZJ, Xu L, Zhang YX, Gao YC (2023). Axial compressive behavior of square concrete-filled steel tube columns with high-strength steel fiber-reinforced concrete. *Engineering Structures*, 285, 116047.

Hussein LF, Al-Taai AAS, Khudhur ID (2020). Sustainability achieved by using voided slab system. *AIP Conference Proceedings*, 2213(1), 020071.

IQS No. 5 (2019). Iraqi specification no. 5: Portland cement. Central Organization for Standardization and Quality Control, Baghdad, Iraq.

Kandil K, El-Shami M, Hekal GM, ElGouhary OM (2025). Behavior of multi-cell steel columns under impact loading. *Challenge Journal of Concrete Research Letters*, 16(2), 95-114.

Lai B, Liew JYR, Hoang AL (2019). Behavior of high strength concrete encased steel composite stub columns with C130 concrete and S690 steel. *Engineering Structures*, 200, 109743.

Lai B, Liew JYR, Wang T (2019). Buckling behaviour of high strength concrete encased steel composite columns. *Journal of Constructional Steel Research*, 154, 27-42.

Latief AF (2018). Structural behavior of hybrid reinforced concrete columns. University of Babylon, El-Hille, Iraq.

Liu J, Gao P, Lin X, Wang X, Zhou X, Chen YF (2023). Experimental assessment on the size effects of circular concrete-filled steel tubular columns under axial compression. *Engineering Structures*, 275, 115247.

Mao WJ, Wang WD, Zhou K, Du EF (2021). Experimental study on steel-reinforced concrete-filled steel tubular columns under the fire. *Journal of Constructional Steel Research*, 185, 106867.

Mohammed AH, Yassin LAG, Hamid MM (2022). Experimental investigation on the ultimate capacity of rectangular reinforced hybrid concrete columns under axial load. *International Journal of GEOMATE*, 23(95), 112-118.

Mohammed Ali TK (2020). Experimental behavior and analysis of hybrid low-high strength reinforced concrete columns. *Journal of Materials and Engineering Structures*, 7(2), 203-214.

Mufja GF (2024). Experimental evaluation of hybrid reinforced concrete columns under eccentric loads externally strengthened with carbon fibre reinforced polymer. University of Babylon, El-Hille, Iraq.

Patel VI, Liang QQ, Hadi MNS (2020). Numerical simulations of circular high strength concrete-filled aluminum tubular short columns incorporating new concrete confinement model. *Thin-Walled Structures*, 147, 106492.

Polat E, Karaman G (2025). Predicting shear strength in reinforced concrete deep beams through finite element modeling of diverse concrete materials. *Challenge Journal of Structural Mechanics*, 11(1), 24-41.

Resheq A (2018). Behaviour of hybrid concrete columns under axial compression loads. *MATEC Web of Conferences*, 162, 1-6.

Richart FE, Brown RL (1934). An investigation of reinforced concrete columns. Engineering Experiment Station, University of Illinois, Urbana, IL, USA.

Rong B (2023). Study on axial compression behavior of 7A04-T6 concrete-filled aluminum tubular columns. *Journal of Building Engineering*, 76, 107118.

Sancıoğlu S, İlgün A, Çarbaş S (2025). Experimental performance analysis of concrete-filled steel column to concrete-filled steel beam connections. *Challenge Journal of Concrete Research Letters*, 16(4), 215-224.

Shaheen YBI, Etman ZA, Sabiha HL (2025). Design of reactive powder concrete mortar mixes through high strength and durability. *Challenge Journal of Concrete Research Letters*, 16(3), 142-154.

Wang FC, Zhao HY, Han LH (2019). Analytical behavior of concrete-filled aluminum tubular stub columns under axial compression. *Thin-Walled Structures*, 140, 21-30.

Xie F, Chen J, Yu QQ, Dong X (2019). Behavior of cross arms inserted in concrete-filled circular GFRP tubular columns. *Materials*, 12(14), 2280.

Xu W, Zhang J, Liu F, Ma Z (2024). Axial compression behavior of assembled aluminum alloy-concrete-carbon steel double-skin tubular column. *Structures*, 69, 107278.

Yıldız Y, Şermet F (2025). Impact of composite columns on soft and weak storey irregularities in buildings without ground floor infill walls. *Challenge Journal of Structural Mechanics*, 11(2), 70-81.

Yuan F, Cao L, Li H (2022). Axial compressive behaviour of high-strength steel spiral-confined square concrete-filled steel tubular columns. *Journal of Constructional Steel Research*, 192, 107245.